Acta Biochim Biophys Sin 2025, 57(x): 1–15
https://cstr.cn/32197.14.abbs.2025130
https://doi.org/10.3724/abbs.2025130
Original Article

Original Article

Autophagy-dependent sensitization effects of PARP inhibitors on recurrent nasopharyngeal carcinoma treated with carbon ion and photon irradiation

Ziyu Le[1,2,3], Haojiong Zhang[1,2,3], Li Chen[1,2,3], Wanzun Lin[1,2,3], Qingting Huang[1,2,3], Shikai Geng[1,2,3], Wei Hu[1,2,3], Huaiyuan Chen[1,2,3], Fangzhu Wan[1,2,3], Xingyu Liu[1,2,3], Jiyi Hu[1,2,3], Fengtao Su[2,4], Jiade J. Lu[5], and Lin Kong[1,2,3,*]

[1]Department of Radiation Oncology, Shanghai Proton and Heavy Ion Center, Fudan University Cancer Hospital, Shanghai 201315, China, [2]Shanghai Key Laboratory of Radiation Oncology, Shanghai 201321, China, [3]Shanghai Engineering Research Center of Proton and Heavy Ion Radiation Therapy, Shanghai 201321, China, [4]Cancer Institute, Fudan University Shanghai Cancer Center, Shanghai Medical College of Fudan University, Shanghai, China, and [5]Department of Radiation Oncology, Proton and Heavy Ion Center, Heyou Hospital, Foshan 523000, China
*Correspondence address. Tel: +86-18017312533, E-mail: konglinjiang@163.com

Received 11 March 2025 Accepted 8 May 2025 Published 2 September 2025

Abstract

Tumor radioresistance and severe toxicity make reirradiation for recurrent nasopharyngeal carcinoma (NPC) a significant clinical challenge. This study aims to investigate the ability of the poly(ADP-ribose) polymerase (PARP) inhibitor olaparib to sensitize recurrent NPC cells irradiated with photon or carbon ion (C-ion), and to explore the underlying mechanism of the synergistic promotion of cell death by olaparib and ionizing radiation. The results show that olaparib has significant X-ray and C-ion radiosensitization effects on recurrent NPC cells and the associated HK-RR photon-resistant model. Radiation, particularly C-ion exposure, induces a homologous recombination (HR)-deficient gene signature in HR-proficient NPC cells, potentially increasing their sensitivity to PARP inhibition. C-ion and X-ray irradiation induces similar modes of cell death, and multiple cell death pathways (including apoptosis, necrosis, ferroptosis, senescence, and autophagic cell death (ACD)) contribute to the cytotoxic effects of radiation combined with olaparib, with ACD being the dominant pathway. Both the pharmacological and genetic inhibition of autophagy significantly attenuate the radiosensitization effect of olaparib. In conclusion, olaparib effectively sensitizes recurrent NPC cells to both X-ray irradiation and C-ion irradiation, with autophagy playing a central role in mediating this effect.

Key words recurrent nasopharyngeal carcinoma, PARP inhibitor, radiosensitivity, cell death, autophagy

Introduction

Approximately 10%–15% of nasopharyngeal carcinoma (NPC) patients experience local recurrence after their primary treatment, for which reirradiation is the main approach [1]. Most local failures occur in the high-dose zone [2], indicating that these recurrences are largely resulted from radioresistance. However, because these radioresistant tumors are surrounded by critical organs at risk that have already absorbed near-tolerance radiation doses, reirradiation is a challenge and is typically associated with poor survival rates and severe toxicity. Compared with conventional photon-based radiation, carbon ion radiotherapy (CIRT) has a better dose distribution, higher linear energy transfer (LET) and greater relative biological effectiveness (RBE), which enables better tumor killing with superior sparing of adjacent organs [3]. These dosimetric and radiobiological advantages make CIRT a promising treatment for local failure disease [4]. Hu *et al.* [5] reported that CIRT used as salvage therapy resulted in 83.7% 2-year overall survival, 58% local control, and 87.3% regional control among 206 patients with locoregionally recurrent NPC. Although the severe toxicities reported in that study were significantly lower than the historical results obtained for reirradiation with photons, 33 patients (16%) developed mucosal necrosis (including ten fatal hemorrhages).

Additional efforts are needed to explore more effective and safer treatment strategies for recurrent NPC.

Combining effective radiosensitizers during treatment may enhance therapeutic outcomes without increasing the radiation dose. The poly(ADP-ribose) polymerase (PARP) family comprises a group of nuclear proteins that are activated upon binding to damaged DNA, thereby playing key roles in the DNA damage response (DDR), with PARP1 being the most extensively studied family member. PARP1 functions primarily to detect single-strand DNA breaks (SSBs) and double-strand DNA breaks (DSBs), as well as to recruit DNA repair machinery and stabilize replication forks during repairs [6]. PARP inhibitors (PARPis) are best known for their synthetic lethality effects with homologous recombination (HR) deficiencies, particularly pathogenic BRCA1 or BRCA2 (BRCA1/2) mutations.

In addition to their use as single agents, PARPis have been shown to be effective radiosensitizers to photon irradiation for various tumor types [7–10]. The radioenhancement ratio varies depending on several factors, such as the drug concentration, experimental design, and tumor cell line. Research on the combination of PARPis with CIRT remains sparse, with significant sensitization effect variations across different models [11–14]. For example, in chondrosarcoma, olaparib significantly sensitizes CH2879 cells to both photon and carbon ion (C-ion) irradiation [11], whereas in OUMS27 and JJ012 cells, sensitization is observed with photons but not with C-ions [12]. Moreover, in osteosarcoma and non-small cell lung carcinoma cells, olaparib has stronger radiosensitizing effects with C-ions than with X-rays.

In the NPC field, investigations of PARPis have been limited. Chow *et al.* [15] reported that olaparib has synergistic effects with photon radiation in several NPC cell lines, including CNE2, HONE1 and HNE1. To date, no studies have explored the sensitization effects of PARPis in NPC or recurrent NPC treated with CIRT, despite the pressing clinical need for such research. In this study, we investigated the effects of PARPis on the sensitization of recurrent NPC to photon and C-ion irradiation. Additionally, we explored the underlying synergistic cell death mechanisms induced by the combination of PARPi and ionizing radiation (IR), with a particular emphasis on the modalities of cell death.

Materials and Methods

Cell culture and cell line authentication

HK-1 cell line, derived from NPCs that recurred at the original site after radiotherapy [16], was obtained from Sun Yat-sen University Cancer Center (Guangzhou, China). The primary NPC cell line C666-1 was procured from MeisenCTCC (Jinhua, China). HK-1 and C666-1 cells were cultured in RPMI 1640 medium (A1049101; Gibco, Waltham, USA) supplemented with 10% fetal bovine serum (10099141C; Gibco) and 50 U/mL penicillin-streptomycin (15070063; Gibco). Cell line authentication was conducted by Genetic Testing Biotechnology (Suzhou, China) via short tandem repeat (STR) analysis (the results are shown in Supplementary Data).

To establish a radioresistant cell model, HK-1 cells were subjected to intermittent X-ray irradiation with a single-dose sequence of 2 Gy–2 Gy–2 Gy–4 Gy–4 Gy–4 Gy–6 Gy–6 Gy–6 Gy–8 Gy–8 Gy–8 Gy–10 Gy–10 Gy. The total irradiation dose was 80 Gy. Following each irradiation session, the cells were allowed to recover until stable passage before subsequent X-ray exposure. Upon completion of the 80 Gy radiation regimen, the surviving cells were named HK-RR, and colony formation assays were conducted to assess photon radiation resistance. Maintenance doses of 2 Gy were administered weekly as described in the literature [17].

Reagents and antibodies

PARP inhibitor used in this study was olaparib (S1060; Selleck, Houston, USA). For *in vitro* cell experiments, olaparib was dissolved in dimethyl sulfoxide (DMSO, D2650; Sigma-Aldrich, St Louis, USA) and stored at 10 mM. It was diluted to the indicated concentrations in complete medium before use. Cells in the combination treatment group were pretreated with olaparib 2 h before irradiation and maintained in the presence of the drug for 24 h postirradiation. The control group was treated with 0.05% DMSO. For *in vivo* studies, the dilution scheme of olaparib was as follows: 4% DMSO + 30% PEG300 (S6704; Selleck) + 66% ddH_2O.

Z-VAD-FMK (Z-VAD, S7023), necrostatin-1 (Nec-1, S8037) and 3-methyladenine (3-MA, S2767) were purchased from Selleck, and ferrostatin-1 (Fer-1, 19766S) was obtained from Cell Signaling Technology (CST; Danvers, USA).

Antibodies for western blot analysis were purchased from CST: anti-LC3A/B (4108; 1:1000), anti-ATG5 (12994; 1:1000), anti-β-Actin (4970; 1:1000), anti-GAPDH (5174; 1:1000), anti-CDKN1A/P21 (2947; 1:1000), anti-mouse IgG HRP (7076; 1:1000) and anti-rabbit IgG HRP (7074; 1:1000). pADPr antibody (sc-56198) was purchased from Santa Cruz Biotechnology (Dallas, USA), and its dilution ratio for western blot analysis was 1:200, while that for immunofluorescence (IF) staining was 1:50. Phospho-histone H2A.X (Ser139) antibody (9718; CST) was used at a dilution of 1:1000 for western blot analysis and 1:400 for IF staining. The goat anti-rabbit IgG H&L (Alexa Fluor® 488; ab150077) and goat anti-mouse IgG H&L (Alexa Fluor® 647; ab150115) were purchased from Abcam (Cambridge, UK) and used at a dilution of 1:400 for IF staining.

DNA extraction and genetic mutation detection

Cell genomic DNA was extracted using the TINamp Genomic DNA Kit (DP304; TIANGEN, Beijing, China) following the manufacture's protocol. Next-generation sequencing and bioinformatics analysis for genetic mutation assessment were conducted by Aita Genetics (Shanghai, China). Libraries were prepared using the NEBNext® Ultra™ II DNA Library Prep Kit for Illumina® (E7645L; New England BioLabs, Ipswich, USA) according to the manufacturer's instructions and were sequenced on an Illumina NovaSeq 6000 platform (Illumina, San Diego, USA), using 2 × 150 bp paired-end strategies. The sequencing reads were aligned to the reference sequences of target genes using the Burrows-Wheeler Aligner [18] (version 0.7.17). Realignment and recalibration were performed using the Genome Analysis Toolkit (version 4.1.8) [19], and annotation was conducted using ANNOVAR (http://annovar.openbioinformatics.org/en/latest/) [20]. Interpretation of all variants was conducted following the guidelines of the American College of Medical Genetics and Genomics [21]. Sanger sequencing of p53 gene mutations was performed by BGI Genomics (Shenzhen, China).

C-ion and X-ray irradiation

CIRT was performed via the IONTRIS particle therapy system (Siemens; Forchheim, Germany) at the Shanghai Proton and Heavy

Ion Center, and CIRT planning was performed via the Syngo® treatment planning system (Siemens). The C-ion beam used for cell irradiation is a horizontal beam with an energy of 156.34 MeV/u. CIRT was delivered via pencil beam scanning with a field size of 10 × 20 cm. The average dose rate was 1 Gy/min. Lung phantoms were used to extend the Bragg peak to 5 mm. The mean LET was 50 keV/μm. The cells were placed vertically in the sample holder, and the position was adjusted via laser alignment to ensure that the cell monolayers were positioned in the middle of the extended Bragg peak. For animal irradiation, the width of the extended Bragg peak is 20 mm. The mice were fixed on polymethyl methacrylate plates with adhesive tape and placed sideways and vertically in a mouse irradiation mold. Before irradiation, the position of each mouse was adjusted so that the longitudinal, transverse and sagittal laser alignment was focused on the subcutaneous tumor. EBT3 films that were pasted on the other side of the polymethyl methacrylate plate were used to confirm the accuracy of the irradiation field. An aluminum block was placed in front of the mold to protect important normal tissues.

X-ray radiation was applied to the cells and animals via an X-RAD225 irradiator (Precision X-Ray, Madison, USA) with the following irradiation parameters: voltage, 225 kV; current, 13.3 mA; Cu filter, 1 mm; SSD, 40 cm; and dose rate, 3.198 Gy/min. Mice were anesthetized with isoflurane through a gas anesthesia machine, and normal tissues were protected with lead plates while the tumors were exposed to radiation. The irradiation doses of C-ions and X-rays were all physical.

Cellular assays

To determine short-term cell viability, cells were seeded at an appropriate density in 96-well plates, with 6 replicate wells per group and allowed to attach overnight. Following the indicated treatments, cell viability was measured at the desired time points using the cell counting kit-8 (CK04; Dojindo Laboratories, Kumamoto, Japan) and a BioTek Cytation™ 3 microplate reader (Agilent Technologies, Santa Clara, USA).

Cellular senescence was evaluated by senescence-associated β-galactosidase (SA-β-Gal) staining using a Senescence β-Galactosidase Staining Kit (C0602; Beyotime, Shanghai, China). Cells were seeded into 6-well plates at an appropriate density and treated as indicated. Staining was performed at the specified time points and the blue-stained senescent cells were counted in 10 randomly selected fields under an inverted microscope at 20× magnification. Results are expressed as the average number of positive cells per field.

Western blot analysis

Whole-cell protein lysate preparation and western blot analysis were performed as previously described [22]. In brief, cells were lysed with RIPA buffer (89901; Thermo Fisher Scientific, Waltham, USA) supplemented with 1× protease inhibitor cocktail (78430; Thermo Fisher Scientific). Proteins were separated by 8%–12.5% SDS-PAGE (C671103; Sangon Biotech, Shanghai, China) and electrophoretically transferred to PVDF membranes (ISEQ00010; Millipore, Darmstadt, Germany). After blocking and incubating with primary and secondary antibodies, the protein bands were visualized using SuperSignal chemiluminescent substrate (34577; Thermo Fisher Scientific) and analyzed with a ChemiDoc imaging system (Bio-Rad, Hercules, USA).

Cell clonogenic assay

Cells were trypsinized to generate single-cell suspensions and seeded in triplicate into 6-well plates or T25 flasks at an appropriate density. Cultures were treated with the indicated concentration of olaparib and/or irradiation 24 h after plating and allowed to grow for 10-14 days until visible colonies (> 50 cells per colony under the microscope) were formed. The colonies were fixed with 4% paraformaldehyde (BL539A; Biosharp, Hefei, China) and then stained with crystal violet staining solution (C0121; Beyotime). Colonies were imaged and counted using a GelCount™ colony counter (Oxford Optronix, Oxford, UK). Surviving fractions (SF) were calculated by dividing the plating efficiency of test samples by the plating efficiency of control samples. Curve fitting was performed by GraphPad Prism 10 (version 10.1.1). The survival curves of C-ions were fitted using the multi-target model (Equation 1), and those of X-ray group were fitted using the linear-quadratic (LQ) model (Equation 2).

$$SF = 1 - (1 - e^{-kD})^{N} \quad (1)$$

$$SF = e^{-\alpha D - \beta D^2} \quad (2)$$

The radiobiological parameters included: SF_2 corresponds to the survival fraction at 2 Gy, D_{37} and D_{10} are the radiation doses leading to 37% and 10% survival, respectively. For the LQ model, α is a constant describing the initial slope of the cell survival curve and β is a smaller constant describing the quadratic component of cell killing. For the multitarget model, the parameter D_0 (mean lethal dose, $D_0 = 1/k$) characterizes the final slope of the curve, and Dq (quasithreshold dose, $Dq = D_0 \times \ln(N)$) represents the ability of cells to repair sublethal damage [23]. The relative biological effectiveness (RBE) was calculated as the ratio of D_{10} (X-rays)/D_{10} (C-ions). The sensitizer enhancement ratios (SER) were defined as the ratio of radiation doses required to produce an equivalent effect (10% or 37% cell survival) in the absence or presence of olaparib.

In vivo xenograft model

To establish recurrent NPC xenografts, five-week-old female BALB/C nude mice (20 ± 2 g; Leagene Biotechnology, Beijing, China) were selected, and 100 μL of single-cell suspension containing 1×10^7 HK-1 cells was injected subcutaneously into the left back of each mouse. Mice with tumor volumes of approximatedly 50 mm^3 were randomly assigned to six treatment groups: (a) Olaparib (50 mg/kg daily, intraperitoneal injection (i.p.) for 5 days); (b) Control (equal volume of vehicle i.p. for 5 days); (c) X-control (X-ray irradiation + vehicle control); (d) C-control (C-ion irradiation + vehicle control); (e) X-olaparib (X-rays + olaparib); (f) C-olaparib (C-ions + olaparib). The day of grouping was defined as Day 0 and no significant differences in tumor volume were observed among the groups on Day 0 (Supplementary Figure S1). Olaparib or vehicle was administered daily from Day 0 to 4. X-ray irradiation (8 Gy) and C-ion irradiation (4 Gy) were both delivered as a single dose on Day 1. In the combination treatment group, olaparib was given 2 h before IR delivery. At 48 h post-irradiation, three mice from each group were sacrificed, and the tumors were harvested for IF staining to assess PARP activity and DNA damage. The remaining mice were monitored for tumor growth, with tumor size measured twice weekly using a vernier caliper until Day 60. The volume was calculated according to the formula: $\pi/6 \times \text{length} \times \text{width}^2$. Mice were euthanized when the tumor volume exceeded 1000 mm^3. The

experimental protocol was evaluated and approved by the Animal Care and Use Committee of Shanghai Proton and Heavy Ion Center. All animal experiments were conducted in Laboratory Animal Science of Fudan University Shanghai Cancer Center (approved code: #SYXK-2020-0006).

Hematoxylin-eosin (H&E) and IF staining

After harvesting the tumors, mouse tumor tissues were fixed in formaldehyde (10%) for 24 h, followed by dehydration, permeabilization, wax dipping, paraffin embedding, and sectioning into 4-μm slices. H&E staining was performed using a Hematoxylin and Eosin Staining Kit (C0105S; Beyotime) according to the manufacturer's instructions. For IF staining, tissue sections were deparaffinized and subjected to antigen retrieval using EDTA antigen retrieval solution (C1033; Solarbio, Beijing, China). After blocking with 5% BSA, the sections were incubated with primary antibodies overnight at 4°C. The next day, the sections were washed with PBS and incubated with secondary antibodies at room temperature for 1 h in the dark. The nuclei were stained with DAPI (C1005; Beyotime). The sections were mounted using antifade mounting medium (P0126; Beyotime), and images were captured using an ECLIPSE Ci microscope (Nikon, Tokyo, Japan) and analyzed with CaseViewer software.

For IF staining of cells, cells were seeded at an appropriate concentration in glass-bottom dishes (801001; NEST, Wuxi, China). After overnight attachment, cells were subjected to the indicated treatments. At the desired time points (*e.g.*, 24, 48 or 72 h), the culture medium was removed, and the cells were fixed with 4% paraformaldehyde, permeabilized with Triton X-100 buffer (P0096; Beyotime), and blocked with QuickBlock™ Blocking Buffer (P0260; Beyotime). Antibody incubation was performed as described above. Images were captured using an LSM800 confocal laser scanning microscope and analyzed with ZEN software (Zeiss, Oberkochen, Germany).

Flow cytometry

For flow cytometric analysis of H2AX (pS139) expression, cells were fixed and permeabilized using the Transcription Factor Buffer Set (562574; BD Biosciences, San Jose, USA) according to the manufacturer's protocol and subsequently incubated in 100 μL of Fix/Perm buffer (1×) plus 5 μL of PE mouse anti-H2AX (pS139) antibody (562377; BD) at 2–8°C for 40–50 min protected from light. Unstained cells served as a negative control. After washing with Perm/Wash buffer (1×), the cells were resuspended in stain buffer (554656; BD) and analyzed by flow cytometry. All flow cytometry analyses in this study were performed using a CytoFLEX S flow cytometer (Beckman, Indianapolis, USA).

For cell cycle analysis, cells were fixed in 70% ethanol overnight at –20°C. The fixed cells were washed twice with cold PBS and then stained with FxCycleTM PI/RNase Staining Solution (F10797; Thermo Fisher Scientific) for 30 min at room temperature in the dark. The samples were analyzed by flow cytometry without additional washing.

Cell apoptosis was assessed using the FITC Annexin V Apoptosis Detection Kit (556547; BD) according to its protocol. Briefly, cells were trypsinized, washed twice with cold PBS and resuspended in 1× binding buffer. Each sample (100 μL) was then incubated with 5 μL of FITC Annexin V and 5 μL of PI for 15 min at room temperature in the dark. After incubation, 400 μL of 1× binding buffer was added to each sample, and flow cytometry analysis was performed. Unstained cells, cells stained with FITC Annexin V alone and cells stained with PI alone were used to establish compensation settings and quadrant gating.

Cell necrosis was assessed by evaluating cell membrane integrity, as described in previous studies [24,25]. The indicated cell samples were stained with 5 μL of PI, and the remaining steps were performed as described for apoptosis analysis.

Cell ferroptosis was determined by measuring intracellular lipid peroxidation [26]. Cells were incubated in fresh medium containing 2 μM BODIPY™ 581/591 C11 (D3861; Thermo Fisher Scientific) at 37°C for 30 min, washed with PBS and immediately subjected to flow cytometric analysis.

Autophagy was assessed using the CYTO-ID® Autophagy Detection Kit 2.0 (ENZ-KIT175; ENZO, New York, USA) following the manufacturer's instructions. Briefly, after trypsinization, cells were washed with assay buffer (1×, containing 5% FBS), then incubated in a mixture of 250 μL assay buffer and 250 μL stain buffer for 30 min at 37°C. The stain buffer was prepared by diluting the CYTO-ID® Green detection reagent in assay buffer at a ratio of 1:1000. After incubation, cells were washed with assay buffer and analyzed in the FL1 channel of flow cytometer.

RNA extraction and sequencing

The experiment was performed in biological triplicate. Total RNA from HK-1 cells subjected to different treatments was extracted with an RNA Easy Fast Tissue/Cell Kit (DP451; TIANGEN) following the manufacturer's instructions. The quality and quantity of the RNA were evaluated with a NanoDrop 2000 (Thermo Fisher Scientific). Before constructing the libraries for RNA sequencing (RNA-seq), RNA samples (1 μg) from each group were processed with VAHTS mRNA Capture Beads (N401; Vazyme, Nanjing, China) to enrich polyA+ RNA. Libraries were prepared using the VAHTS mRNA-seq v2 Library Prep Kit for Illumina® (NR601; Vazyme) and were sequenced on an Illumina sequencing platform on a 150 bp paired-end run. The FastQC (v0.11.9) tool (https://www.bioinformatics.babraham.ac.uk/projects/fastqc/) was used for quality control of the raw data, and Trimmomatic [27] (v0.33) was used to remove adapters and low-quality reads. HISAT2 [28] (v2.2.1) was used to align the sequences to the human reference genome (GRCh38/hg38). Read counts per gene/transcript were quantified using featureCounts [29] (v1.6.3). Gene annotation was based on the NCBI RefSeq database (Release 77). Gene expression levels were calculated as fragments per kilobase of transcript per million mapped reads (FPKM) values using R (version 4.1.3).

Supervised cluster analysis and gene set variation analysis (GSVA) were conducted using R. The HRD gene signature, comprising 230 genes, was sourced from the study by Peng *et al* [30]. Gene ID conversion was carried out using the OmicStudio tools (https://www.omicstudio.cn/tool) [31]. Dataset merging and batch effect removal were performed using Sangerbox 3.0 (http://www.sangerbox.com/tool) [32]. Gene sets related to the cell death pathway were downloaded from the GSEA database (http://www.gsea-msigdb.org/gsea/msigdb).

Cell transfection

Autophagic flux was assessed using a tandem fluorescently tagged LC3 probe (GPL2001; GeneChem, Shanghai, China). HK-1 cells were cultured to approximately 50% confluence in 6-well plates and

infected with stubRFP-sensGFP-LC3 lentivirus (MOI = 10) according to the manufacturer's instructions. Stably expressing stubRFP-sensGFP-LC3 cells selected by puromycin (2 μg/mL) were treated with olaparib and/or radiation, and images of the cells were captured at the designated time points using an LSM800 confocal laser scanning microscope.

For *ATG5* knockdown, three human ATG5 shRNA plasmids constructed by GeneChem were used: shATG5-65: 5′-GATTCATG GAATTGAGCCAAT-3′; shATG5-66: 5′-CCTTTCATTCA GAAGCTGTTT-3′; shATG5-67: 5′-CCTGAACAGAATCATCCTTAA -3′. Control cells were transfected with an empty vector (CON207; GeneChem). Plasmids transfection was performed using Lipofectamine™ 3000 (L3000001; Thermo Fisher Scientific). Stable *ATG5*-knockdown cells were selected with puromycin (2 μg/mL) and verified by western blot analysis.

Proteomic analysis

The 4D-Label-free proteomics analysis in this study was conducted by Applied Protein Technology (Shanghai, China). Following protein extraction and digestion, liquid chromatography-tandem mass spectrometry analysis was performed using a NanoElute separation system (Bruker, Billerica, USA) coupled with a timsTOF Pro mass spectrometer (Bruker). Raw mass spectrometry data were processed using MaxQuant (version 1.5.3.17) for protein identification and quantitation. Label-free quantification was conducted across three technical replicates using the LFQ algorithm.

Transmission electron microscopy (TEM)

TEM was conducted with support from Powerful Biology (Wuhan, China). Briefly, cells were collected and incubated in 2.5% glutaraldehyde overnight for primary fixation, then washed at least three times with 100 mM phosphate buffer (pH 7.4) and postfixed in 1% osmium tetroxide and 100 mM phosphate buffer for 2 h. After washing with phosphate buffer, the cells were dehydrated through a graded ethanol series and subjected to resin infiltration and embedding. The embedded samples were sectioned into ultrathin slices (80 nm) using an EM UC7 ultramicrotome (Leica Biosystems, Nussloch, Germany), and stained with 2% uranyl acetate and lead citrate. The images were acquired using an FEI Tecnai transmission electron microscope (Thermo Fisher Scientific).

Statistical analysis

Data analysis and graphing were performed via GraphPad Prism unless otherwise specified. Two-tailed *t* tests were used for statistical comparisons between two groups, one-way ANOVA was used for multigroup comparisons, and two-way ANOVA was used for comparisons of dose-response curves. For *in vivo* tumor growth delay, the time to reach 1000 mm^3 was assessed via Kaplan-Meier analysis and the log-rank test. $P < 0.05$ was considered to indicate statistical significance.

Results

Sensitization effect of olaparib on X-ray and C-ion irradiation *in vitro*

The cytotoxic effect of olaparib alone was evaluated first. Next-generation sequencing revealed no loss-of-function variants in HR-related genes (Supplementary Table S1) in the HK-1 cell line (details in Supplementary Table S2). Consistent with this genetic background, olaparib monotherapy demonstrated limited cytotoxicity against HK-1 cells. Viability assays revealed that cytotoxicity was closely associated with the duration of drug exposure. The IC_{50} values of olaparib in HK-1 cells decreased with increasing exposure time, with values of 224.5 μM at 24 h, 124.2 μM at 48 h, and 73.25 μM at 72 h (Figure 1A). As shown in Figure 1B, compared with primary C666-1 NPC cells, recurrent NPC cells presented greater resistance to X-rays ($P = 0.0015$). Both cell lines showed increased sensitivity to C-ions relative to X-rays. The relative biological effectiveness at 10% cell survival (RBE_{10}) for HK-1 cells was calculated to be 1.79. For the subsequent experiments, an RBE value of 2 was used to determine the equivalent biological dose.

The enzymatic activity of PARP was evaluated by detecting the accumulation of poly(ADP-ribose) (PAR), which is the product of PARP activation. A significant accumulation of PAR chains was observed following both X-ray and C-ion irradiation. Pretreatment with olaparib at concentrations ranging from 1–10 μM, which are well below the IC_{50} values, effectively inhibited radiation-induced PARP activity (Figure 1C). Clonogenic assays revealed that olaparib, at concentrations of 1, 5 or 10 μM, enhanced the radiosensitivity of HK-1 cells to both X-rays and C-ions. The sensitizer enhancement ratios at 10% cell survival (SER_{10}) for X-rays were 1.22, 1.53, and 1.69, respectively, and the SER_{10} values for C-ions were 1.29, 1.55, and 1.67, respectively (Figure 1D,E). The detailed radiobiological parameters of the multitarget and LQ models are provided in Table 1. An olaparib concentration of 5 μM was selected for subsequent *in vitro* studies. Additionally, we evaluated the radiosensitizing effect of PARPis on primary NPC cells (C666-1), and the results are presented in Supplementary Figure S2.

To further investigate the sensitizing effects of olaparib on radioresistant recurrent NPC cells, we established a photon-resistant cell model based on HK-1 cells (HK-RR). Clonogenic experiments demonstrated a significant reduction in X-ray radiosensitivity in HK-RR cells relative to HK-1 cells (Figure 1F; $P = 0.0019$). However, the difference in C-ion sensitivity between the two cell lines was minimal (Figure 1G; $P = 0.60$), suggesting that C-ions may offer a therapeutic advantage in photon-resistant cells. Moreover, treatment with 5 μM olaparib significantly enhanced the sensitivity of HK-RR to both X-rays and C-ions, with SER_{10} values of 1.58 for X-rays and 1.66 for C-ions (Figure 1F,G), indicating its potential therapeutic value in radioresistant recurrent NPC. Representative clonogenic images of HK-1 and HK-RR cells irradiated with X-rays or C-ions, with or without olaparib treatment, are presented in Figure 1H,I. Additional radiobiological parameters, including SER_{37} and SF_2, are provided in Supplementary Table S3.

Olaparib combined with ionizing radiation suppresses tumor growth in HK-1 xenograft models

We next evaluated the *in vivo* radiosensitizing efficacy of olaparib in a nude mouse subcutaneous xenograft tumor model. The mice were treated with olaparib and/or IR (Figure 2A). The mice that received X-ray or C-ion irradiation alone were given the vehicle control and were grouped into the X-control and C-control groups, respectively. At 48 h postirradiation, the intratumoral PAR expression in the olaparib combination treatment group was significantly lower than that in the C-control group, confirming that olaparib effectively inhibits PARP activity *in vivo* (Figure 2B). The tumor growth curves produced for each treatment group are shown in Figure 2C. The tumor volumes were measured twice a week until

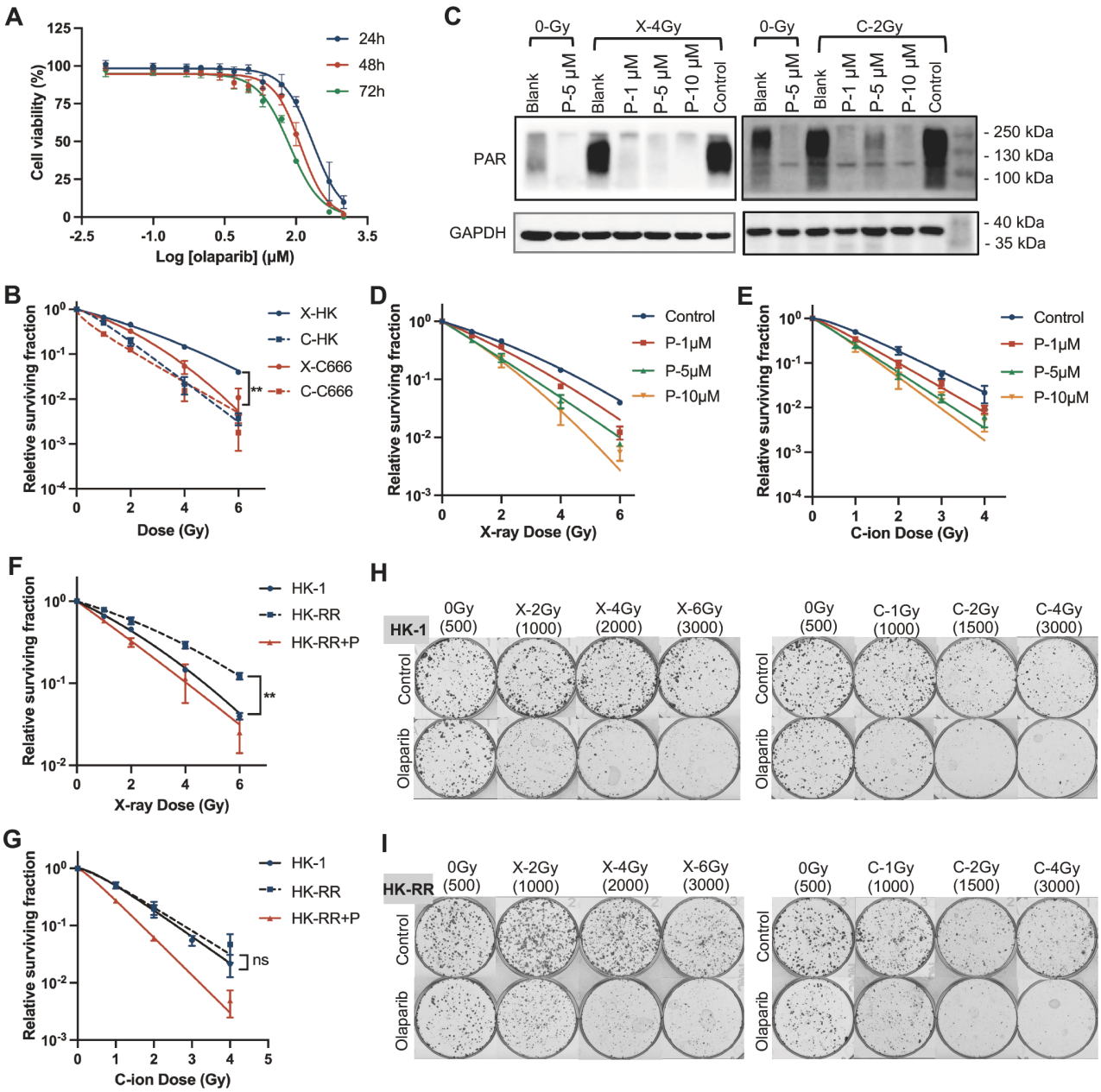

Figure 1. Olaparib increases the radiosensitivity of recurrent NPC cells to X-rays and C-ions (A) HK-1 cells were exposed to different concentrations (0.01–1000 μM) of olaparib for 24–72 h, and the cytotoxicity of olaparib was measured via CCK-8 assay, with cell viability expressed as a percentage of that of the vehicle-treated (0.05% DMSO) control. (B) Survival curves of C666-1 and HK-1 cells following exposure to X-ray or C-ion irradiation, with the values normalized against those of the nonirradiated group. (C) The effects of olaparib at concentrations ranging from 0 to 10 μM on PARP activity were assessed in HK-1 cells at 24 h postirradiation with 4 Gy of X-rays or 2 Gy of C-ions. Protein loading was evaluated via the use of GAPDH. (D,E) Clonogenic survival curves of HK-1 cells treated with 0–10 μM olaparib in combination with X-ray (D) or C-ion (E) irradiation. The surviving fractions were normalized to the corresponding nonirradiated control at each drug concentration. (F,G) The radiosensitivities of HK-RR cells and parental HK-1 cells to X-rays and C-ions, with or without olaparib (5 μM), were assessed via clonogenic survival assays. All values were normalized to those of the nonirradiated group. (H,I) Representative clonogenic images of HK-1 (H) and HK-RR cells (I) irradiated with X-rays or C-ions, with or without olaparib (5 μM) treatment. The numbers in parentheses indicate the number of cells plated per well within each dose group. Each assay was repeated three times. Data are presented as the mean ± SD. $^{**}P < 0.01$. HK-RR + P denotes the HK-RR group treated with olaparib.

Day 60, and the mice were euthanized when the tumor volume reached or exceeded 1000 mm^3, which was defined as a Kaplan-Meier event.

The first euthanasia event occurred on Day 34. The tumor growth curves obtained for the mean tumor volume of each group up to day 34 are presented in Figure 2D. No statistically significant differences in mean tumor volume were observed on day 34 between the control group and either the olaparib monotherapy group ($P = 0.43$)

Table 1. Radiobiological parameters of HK-1 cells subjected to photon or carbon ion irradiation in the presence or absence of olaparib

Model	Parameter	X-ray				C-ion			
		Control	Olaparib (1 μM)	Olaparib (5 μM)	Olaparib (10 μM)	Control	Olaparib (1 μM)	Olaparib (5 μM)	Olaparib (10 μM)
Multi-target	k	0.52	0.60	0.74	1.01	1.08	1.28	1.44	1.63
	N	1.25	1.11	1.00	1.63	1.66	1.30	1.09	1.27
	D_0	1.94	1.67	1.35	0.99	0.93	0.78	0.70	0.61
	D_q	0.44	0.18	0.00	0.48	0.47	0.20	0.06	0.15
	SER_{37}	–	1.29	1.75	1.61	–	1.41	1.84	1.84
	SER_{10}	–	1.22	1.57	1.78	–	1.29	1.55	1.67
	SF_2 (%)	42.46	32.90	22.83	20.73	18.40	10	6.16	4.82
LQ	α	0.36	0.50	0.73	0.69	0.58	0.99	1.34	1.35
	β	0.03	0.03	0.01	0.05	0.12	0.07	0.02	0.07
	SER_{37}	–	1.28	1.73	1.77	–	1.42	1.82	1.89
	SER_{10}	–	1.22	1.53	1.69	–	1.27	1.54	1.64
	SF_2 (%)	43.54	33.45	22.76	20.71	19.20	10.29	6.24	4.99

LQ, linear-quadratic.

or the X-control group ($P = 0.70$; Figure 2E). However, C-ion irradiation significantly inhibited tumor growth ($P = 0.02$ for comparisons with both the control group and the X-control group; Figure 2E). The tumor volume in the olaparib combination treatment group was lower than that in the irradiation alone group ($P = 0.02$ for the comparison between X-control and X-olaparib; Figure 2E). Finally, the results of the Kaplan-Meier analysis were consistent with the observations on Day 34. Neither olaparib monotherapy ($P = 0.07$) nor X-rays alone ($P = 0.45$) had significant inhibitory effects on tumor growth relative to that of the control group (Figure 2F). In contrast, C-ions, at equal biological doses, were significantly more effective than X-rays in suppressing tumor growth in the HK-1 xenograft models ($P = 0.0017$ in comparison with the control group; Figure 2F). These findings highlight the therapeutic advantage of C-ions over X-rays in reirradiation for recurrent NPC. Furthermore, olaparib combined with either X-ray or C-ion radiation resulted in greater tumor growth inhibition than IR alone did ($P = 0.03$ for the comparison between X-control and X-olaparib; $P = 0.01$ for the comparison between C-control and C-olaparib; Figure 2F). In regions where CIRT is not readily accessible, photon-based reirradiation combined with olaparib may offer enhanced therapeutic benefits for recurrent NPC.

Olaparib combined with ionizing radiation impairs the DNA damage repair process

Since PARP plays key roles in the DDR pathway, inhibiting PARP impairs the ability to repair radiation-induced DNA damage, resulting in increased cell death. This mechanism partly underlies the radiosensitizing effects of PARPis. In this study, we evaluated DNA damage across different treatment groups and monitored its dynamic changes over time via IF staining (Figure 3A) and flow cytometry (Figure 3B–D). Olaparib monotherapy did not notably induce DSBs in HK-1 cells, which was consistent with the intact HR functionality of these cells. At 1 h postirradiation, a substantial number of γ-H2AX foci were observed in both the single-radiation groups and the olaparib combination groups (Figure 3A), with flow cytometry quantification revealing no significant difference between the two groups (Figure 3B; $P > 0.99$). However, at 24 and 48 h postirradiation, the combination group presented significantly more γ-H2AX-positive cells than the single-radiation groups did, and this difference was more obvious in the photon radiation group (Figure 3A,C,D). Consistently, in the xenograft models, the combination treatment group presented more and larger γ-H2AX foci in tumor tissues than did the C-ion-alone group at 48 h postirradiation (Figure 3E). These findings suggest that while radiation induces comparable levels of initial DNA damage with or without olaparib, the combination treatment results in more unrepaired DNA lesions persisting up to 48 h postirradiation due to impaired repair processes.

Following DNA damage, cell cycle arrest is promptly initiated alongside DNA repair processes. Consistent with the above results, the addition of olaparib further increased the proportion of cells undergoing G2/M phase arrest and prolonged the duration of arrest following X-ray or C-ion irradiation (Figure 3F). Even at 72 h postirradiation, the fraction of cells arrested in the G2/M phase in the combined treatment group remained significantly greater than that in the single-radiation groups (Figure 3F, X-rays, $P = 0.003$; C-ions, $P = 0.03$).

Sizemore *et al.* [33] reported that radiation induces the export of BRCA1 from the nucleus to the cytoplasm, resulting in decreased HR repair rates and increased PARPi cytotoxicity in breast tumor cells. This finding suggests a potential mechanism by which radiation may promote the development of an HR-deficient (HRD) phenotype, thereby sensitizing cells to PARPis. Peng *et al.* [30] identified an HRD gene signature on the basis of transcriptional profiling that can functionally assess HR repair status. With this method, we performed transcriptome analyses of HK-1 cells and used supervised clustering to determine whether radiation affects HR functionality. Consistent with the HR-related gene mutation results, the unirradiated HK-1 cells (the control and olaparib monotherapy groups) clustered with the HR-intact group (Figure 3G). In contrast, cells treated with radiation, especially those treated with C-ions, presented a gene signature similar to that of the HRD group (Figure 3G). These results support our hypothesis that radiation exposure induces an HRD phenotype in HR-intact NPC cells. However, further studies are needed to verify this hypothesis.

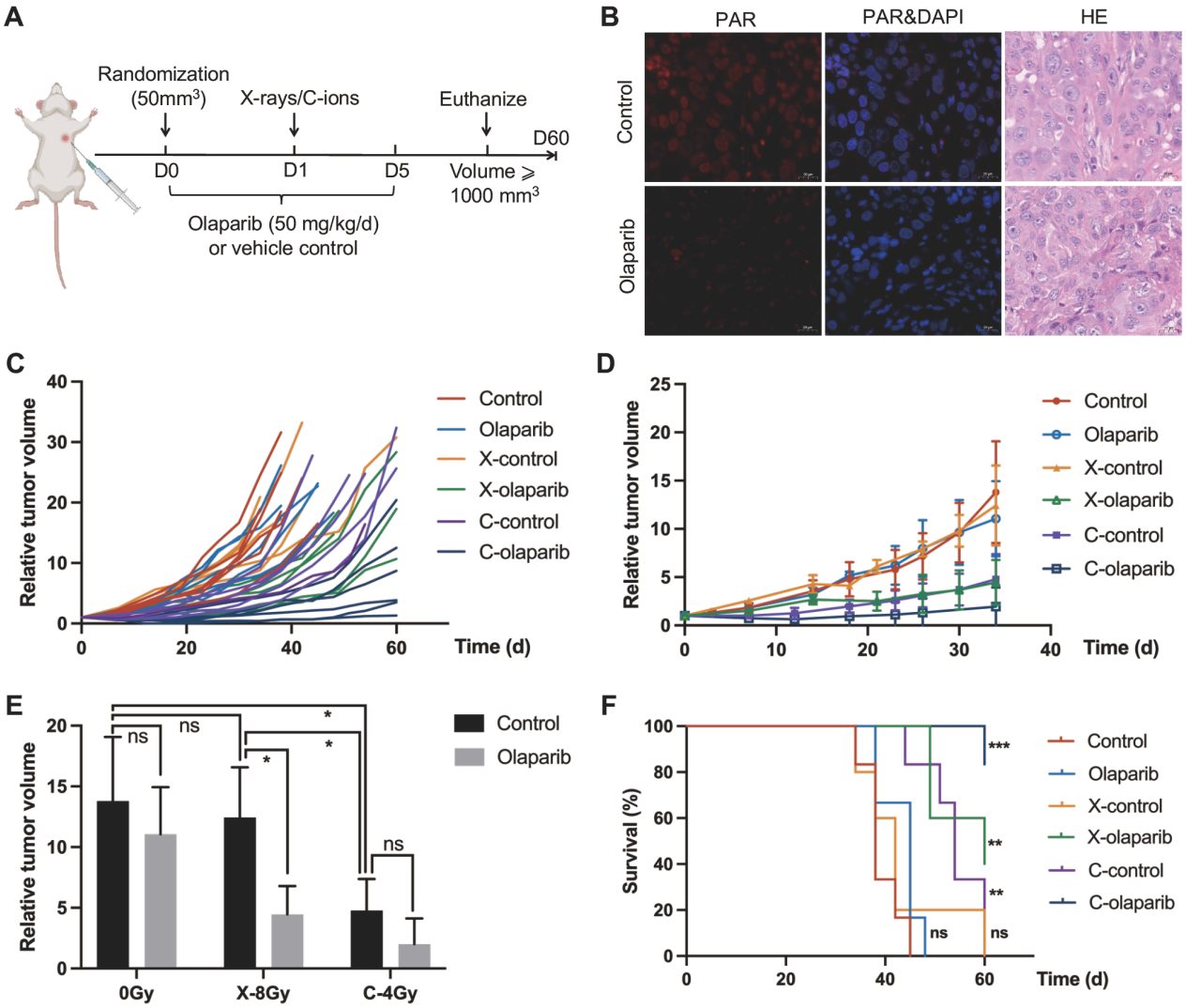

Figure 2. Olaparib combined with ionizing radiation effectively inhibits HK-1 xenograft tumor growth (A) Overview of the *in vivo* experiments. (B) Intratumoral PAR expression in mice treated with CIRT alone (upper) or CIRT combined with olaparib (lower) was assessed at 48 h post-irradiation (40× magnification, scale bar: 20 μm). H&E staining and IF staining were performed on serially sliced paraffin sections (4-μm thickness) as a reference for tumor positioning. (C) Tumor growth curves produced for each treatment group ($n = 6$ for the control, olaparib, C-control and C-olaparib groups; $n = 5$ for the X-control and X-olaparib groups). The control and olaparib groups represent the nonirradiated groups. The tumor volumes are presented relative to the tumor volume of each mouse on Day 0. (D) Tumor growth curves showing the mean tumor volume for each group up to day 34. (E) The average tumor volume of each group on day 34. (F) Kaplan-Meier curves produced for each treatment group. The log-rank (Mantel-Cox) test results presented in the figure were used to compare each treatment group with the control group. $^{*}P < 0.05$, $^{**}P < 0.01$, and $^{***}P < 0.001$.

Olaparib combined with IR activates various modes of cell death

Radiation-induced DNA damage affects multiple cell fate decisions to kill tumor cells and achieve therapeutic effects [34]. To investigate how the combination treatment enhances cell death, we performed proteomic and transcriptomic analyses on cells subjected to different therapies. GSVA revealed that both the radiation type and the combined treatment activated multiple cell death pathways, including pathways related to apoptosis, necrosis, autophagy, ferroptosis, and cell senescence (Figure 4A,B). The transcriptome data revealed the activation of cell senescence, apoptosis, and autophagy at 1 h postirradiation, with necrosis and ferroptosis showing more pronounced enrichment levels at 24 h after IR (Figure 4A). Moreover, the enrichment patterns of the cell death modes differed slightly between C-ions and X-rays. Cell senescence and ferroptosis were more prominent in the X-ray group, whereas apoptosis and autophagy were more prevalent in the C-ion group. The proteomics-based GSVA results generally aligned with the transcriptome findings, with particularly notable autophagy and necrosis enrichment observed in the C-ion + olaparib combination group (Figure 4B).

To further validate the GSVA findings, the levels of these five types of cell death were assessed in cells treated with olaparib and/or radiation. Apoptosis (Figure 5A,B), necrosis (Figure 5C,D), and ferroptosis (Figure 5E,F) were assessed via flow cytometry. Autophagy levels were determined through western blot analysis

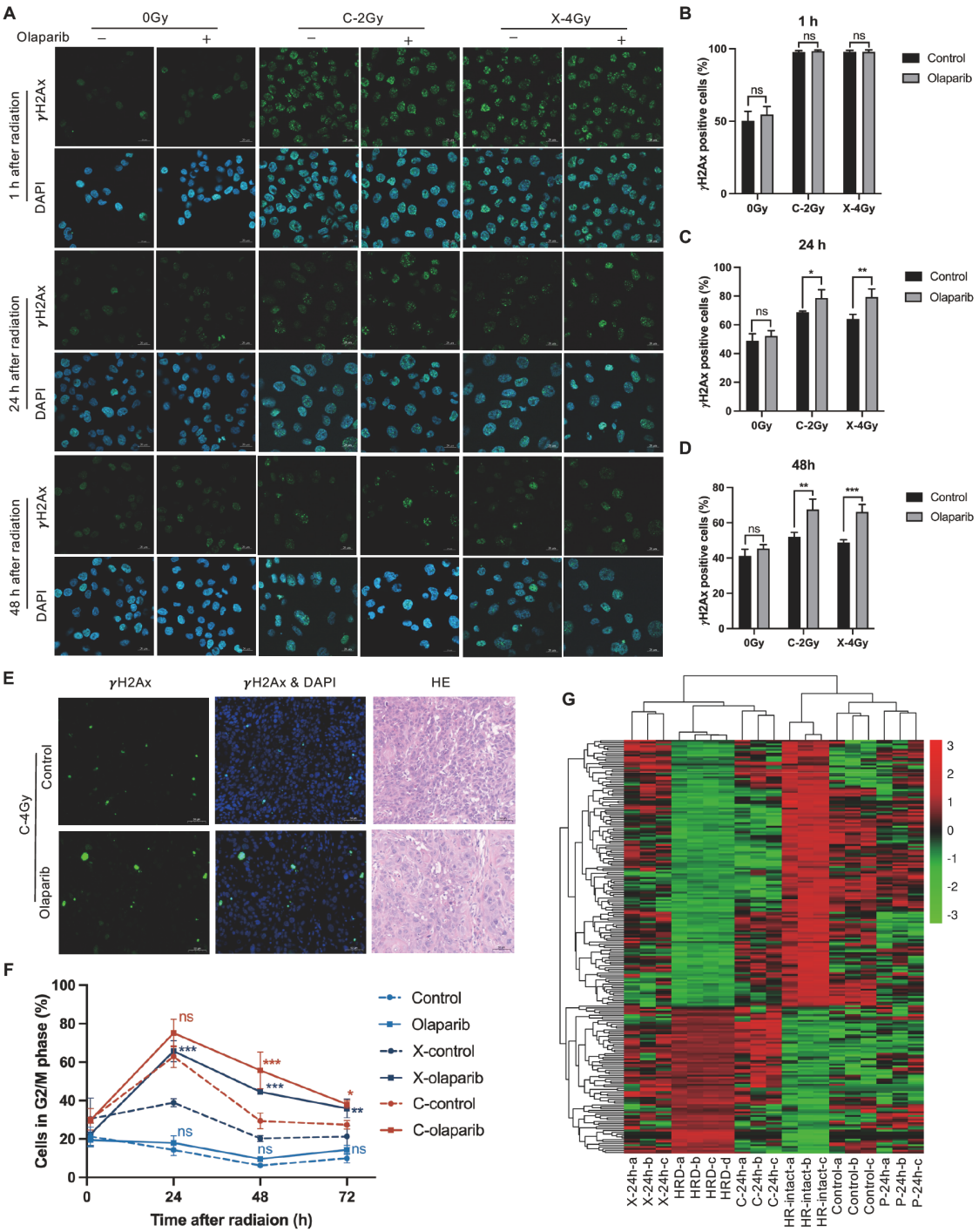

Figure 3. The combination of radiation and olaparib increases the amount of unrepaired DNA damage (A) IF staining results obtained for γ-H2AX in HK-1 cells following different treatments at three time points. (40× magnification, scale bar: 20 μm). Olaparib was used at a concentration of 5 μM. (B,C,D) Quantification of γ-H2AX levels by flow cytometry analysis in each treatment group at the indicated time points. (E) Intratumoral γ-H2AX foci in mice treated with CIRT, with or without olaparib, were assessed at 48 h postirradiation (40× magnification; scale bar: 50 μm). (F) Percentage of cells in the G2/M phase in each treatment group at 1–72 h postirradiation. The *t* test results presented in the figure represent comparisons between the olaparib-treated groups and their corresponding control groups within each radiation treatment group (0 Gy, X-rays, C-ions) at the indicated time points. The flow cytometry results detailing the specific cell cycle distribution are illustrated in Supplementary Figure S3. Data are presented as the mean ± SD of three independent experiments. (G) The gene expression data of HK-1 cells treated with 4 Gy of X-rays (X-24 h), 2 Gy of C-ions (C-24 h), 5 μM olaparib (P-24 h) or the blank control (Control) were used to assess HR repair status via supervised clustering analysis. HRD-a, b, c, and d represent the HRD reference group, and HR-intact-a, b, and c denote the HR-intact reference group. The gene expression data of these two groups corresponded to those of the Brit1 group and CT0A group, respectively, in the study by Peng G *et al.* [19], and they can be downloaded from the Gene Expression Omnibus Database (accession code GSE54296). $^{*}P < 0.05$, $^{**}P < 0.01$, and $^{***}P < 0.001$.

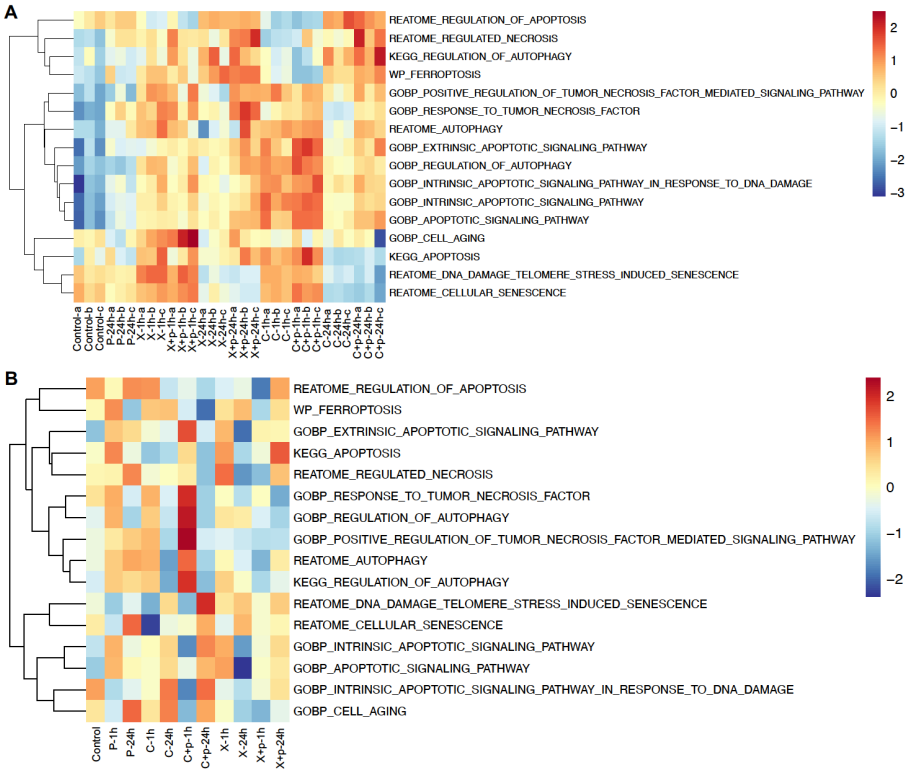

Figure 4. Olaparib combined with IR activates various cell death pathways GSVA heatmaps of the cell death pathway based on the transcriptome (A) and proteome data (B) of HK-1 cells. The group names are as follows: P-1 h or P-24 h (continuous incubation with 5 μM olaparib for 1 h or 24 h, respectively), X-1 h or X-24 h (4 Gy of X-rays, sampled at 1 h or 24 h postirradiation, respectively), X + p-1 h or X + p-24 h (4 Gy of X-rays + olaparib, sampled at 1 h or 24 h postirradiation, respectively), C-1 h or C-24 h (2 Gy of C-ions, sampled at 1 h or 24 h postirradiation, respectively), and C + p-1 h or C + p-24 h (2 Gy of C-ions + olaparib, sampled at 1 h or 24 h postirradiation, respectively).

of the soluble (LC3-I) and membrane-bound (LC3-II) forms of LC3B (Figure 5G), as well as TEM (Figure 5H), RFP-GFP-LC3 fluorescence imaging (Figure 5I), and flow cytometry (Figure 5J,K). Cellular senescence was evaluated by detecting the intracellular accumulation of senescence-associated β-galactosidase (Figure 5L, M) and the P21 protein (Figure 5N). Olaparib alone did not notably affect these five modes of cell death in HK-1 cells. Consistent with the GSVA findings, apoptosis, necrosis, ferroptosis, autophagy, and cellular senescence were activated to varying degrees following X-ray or C-ion exposure. The addition of olaparib further enhanced these cell death pathways, with the most pronounced effects observed at 48 h and 72 h postirradiation (the data observed at 24 h postirradiation are depicted in Supplementary Figure S4).

Autophagy plays a central role in the cell death patterns induced by combination treatment with olaparib and radiation

To further clarify the contribution of each mode of cell death to the cytotoxicity of the combination treatment, coculture experiments with the following cell death inhibitors were conducted: Z-VAD, which is an apoptosis inhibitor; Nec-1, which is a necrosis inhibitor; Fer-1, which is a ferroptosis inhibitor; and 3-MA, which is an autophagy inhibitor. The efficacy of each inhibitor was confirmed, as shown in Supplementary Figure S5. At 48 h postirradiation, reductions in the numbers of cells were observed in the X-ray and C-ion groups, accompanied by increases in the numbers of wide and flat giant cells, pyknotic cells, and cellular debris (Figure 6A). This cell death phenomenon was more pronounced in the olaparib combination treatment groups. The addition of Z-VAD or NEC-1 slightly alleviated cell death but not as significantly as the addition of the autophagy inhibitor did. In both the radiation groups and the combined treatment group, the irradiated cells cocultured with 3-MA exhibited similar cell morphologies and sizes to those of the nonirradiated group (Figure 6A).

The CCK8 survival results (the left panels of Figure 6B,C) were consistent with the observed cell growth morphology. For both X-rays and C-ions, cell death induced by either type of radiation alone or the combined treatment was significantly alleviated by 3-MA, indicating the involvement of autophagic cell death (ACD). The effects of Z-VAD, Nec-1, and Fer-1 on cell survival were minimal, with only Z-VAD showing statistical significance in some groups. Furthermore, the percentage of surviving cells rescued by each inhibitor in the combination treatment groups was calculated and is presented as pie charts in the right panels of Figure 6B,C. ACD was the primary contributor to cell death in both the X-ray + olaparib and C-ion + olaparib combination groups, followed by apoptosis and necrosis. Autophagy inhibition enhanced cell survival by approximately 53.97% and 47.19% in the X-ray + olaparib and C-ion + olaparib groups, respectively. Additionally, ferroptosis con-

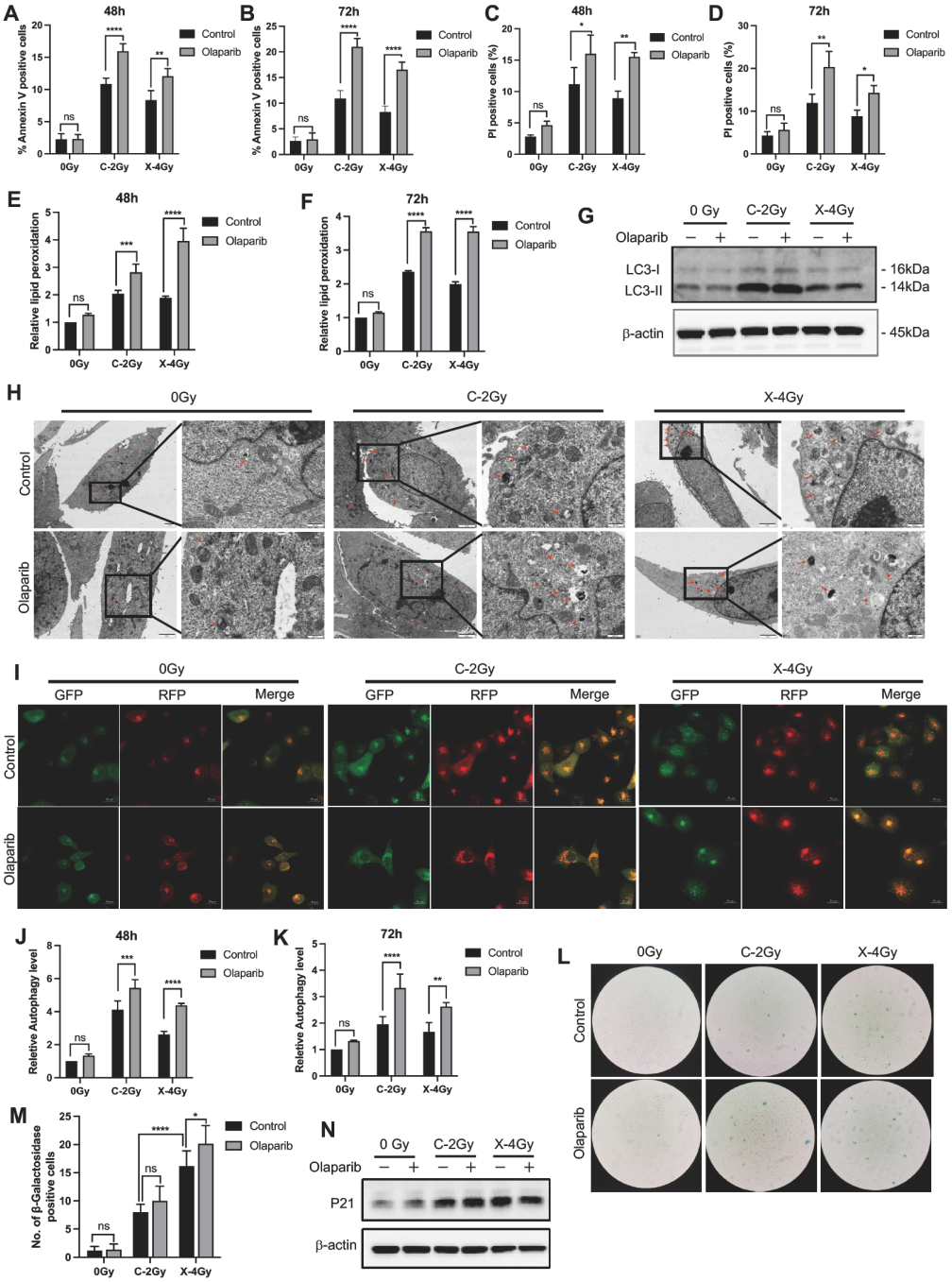

Figure 5. Olaparib combined with IR triggers multiple modes of cell death in HK-1 cells The cells were treated with C-ions (2 Gy) or X-rays (4 Gy) with or without olaparib (5 μM). (A,B) Bar graphs of apoptosis quantified by flow cytometry at 48 h and 72 h postirradiation for each treatment group, and the corresponding dot plot diagrams are shown in Supplementary Figure S4A. Bar graphs of cell necrosis (C,D) and ferroptosis (E,F) quantified by flow cytometry at 48 h and 72 h postirradiation. The data for 24 h postirradiation are shown in Supplementary Figure S4B-D. (G) Western blot analysis of LC3 at 24 h postirradiation, with β-actin as the loading control. (H) Representative TEM microphotographs of HK-1 cells in each group at 24 h postirradiation, with red arrows indicating double-membrane autophagosomes and single-membrane autophagolysosomes (scale bars: 2 μm and 500 nm). (I) Images acquired at 24 h postirradiation from stably expressing stubRFP-sensGFP-LC3 cells treated with olaparib and/or radiation (scale bar: 20 μm). Upon merging, autophagosomes displaying both RFP and GFP signals appeared as yellow puncta. Autophagolysosomes presented attenuated GFP signals due to their acidic environment and appeared as red foci of the RFP signal. (J,K) Autophagic vacuoles were labeled via CYTO-ID® staining at 48 h and 72 h after radiotherapy, and the fluorescence intensity was quantified via flow cytometry. The values were normalized to those of the nonirradiated vehicle-control group. The data for 24 h postirradiation are shown in Supplementary Figure S4E. (L) Representative images of SA-β-Gal staining at 72 h postirradiation. (M) SA-β-Gal-positive senescent cells, identified by blue staining, were counted in 10 random visual fields via an inverted microscope at 20× magnification. The results are expressed as the average number of positive cells per field. (N) Western blot analysis of P21 at 72 h postirradiation. β-actin served as the loading control. Data are presented as the mean ± SD of three independent experiments. $*P < 0.05$, $**P < 0.01$, $***P < 0.001$, and $****P < 0.0001$.

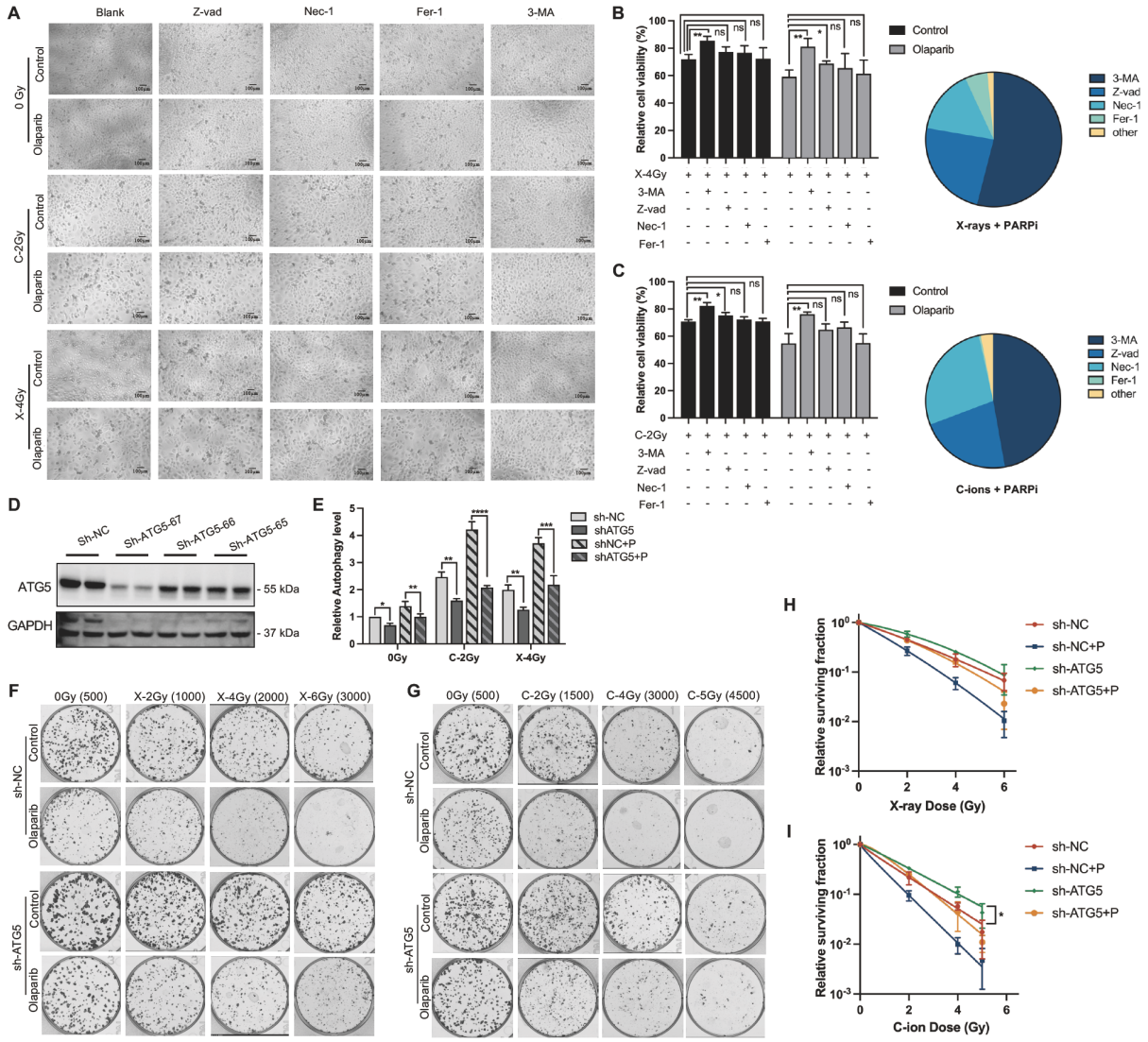

Figure 6. Autophagy inhibition attenuates the radiation-sensitizing effect of olaparib (A) HK-1 cells were plated in 96-well plates and treated with X-ray or C-ion irradiation, with or without olaparib (5 μM), in the presence of different cell death inhibitors. Z-VAD (15 μM), Nec-1 (15 μM) and Fer-1 (5 μM) were added 24 h before radiation exposure, and 3-MA (5 μM) was added 2 h before radiation. All the inhibitors were incubated for 24 h postirradiation. The morphology of the cells was observed and imaged 48 h after irradiation via an inverted microscope (20× magnification; scale bar: 100 μm). (B,C) HK-1 cells were treated as described in (A). Left panel: Cell survival was assessed via CCK-8 assay 48 h after X-ray or C-ion exposure, with the values normalized to those of the nonirradiated control of the corresponding drug group. Right panel: The proportion of surviving cells rescued by each inhibitor in the X-ray + olaparib or C-ion + olaparib combination treatment group was calculated and is presented as a pie chart. The "other" category represents additional cell death mechanisms, determined as one minus the sum of the cell survival fractions rescued by the four inhibitors. (D) The gene knockdown efficiency of three ATG5-targeting shRNAs was confirmed via western blot analysis. GAPDH served as the loading control. Sh-ATG5-67 clones were selected for subsequent studies. (E) Cells transfected with sh-ATG5 or sh-NC were treated with olaparib and/or radiation, and their autophagy levels were measured by flow cytometry 48 h after irradiation. (F,G) *ATG5* knockdown significantly increased the HK-1 cell survival rate following X-ray or C-ion irradiation, with or without olaparib (5 μM). The numbers in parentheses indicate the number of cells plated per well for each dose group. Survival curves were generated for the X-ray (H) and C-ion (I) groups, with the values normalized to those of the nonirradiated group. Data are presented as the mean ± SD. *$P < 0.05$, **$P < 0.01$, ***$P < 0.001$, and ****$P < 0.0001$.

tributed more to cell death in the X-ray group than in the C-ion group, which aligns with the GSVA results of the transcriptome analysis.

To further validate the results of the pharmacological autophagy inhibition experiments, we generated an HK-1 cell line in which *ATG5*, a crucial autophagy-related gene, was knocked down. The efficiency of *ATG5* knockdown is shown in Figure 6D, and sh-ATG5-67 clones were selected for subsequent studies. As shown in Figure 6E, *ATG5* knockdown significantly suppressed both basal autophagy and radiation-induced autophagy relative to those in control vector-transfected cells (sh-NC). The effect of genetic autophagy inhibition on cell survival following X-ray or C-ion exposure, with or without olaparib, was assessed through clonogenic assays (Figure 6F,G), and the corresponding survival curves are shown in Figure 6H,I. Autophagy inhibition reduced cell radiosensitivity, as evidenced by the presence of more surviving

colonies and higher SF_2 values in the sh-ATG5 group than in the sh-NC group after X-ray or C-ion exposure. Specifically, the SF_2 values for the sh-ATG5 group following X-ray irradiation and C-ion irradiation were 57.87% and 31.55%, respectively, whereas they were 48.56% and 24.74%, respectively, for the sh-NC group. Significant differences were observed in the survival curves produced for the C-ions between the two groups (Figure 6I, P = 0.02). Importantly, autophagy inhibition notably attenuated the radiosensitizing effect of olaparib. The SER_{10} values of olaparib for X-rays and C-ions in the sh-NC cells were 1.56 and 1.57, respectively, whereas these values in the sh-ATG5 cells decreased to 1.23 and 1.34, respectively. These results suggest that ACD is involved in radiation-induced cell death and that autophagy is the dominant cell death pathway in olaparib combination therapy.

Discussion

Performing reirradiation to treat locally recurrent NPC is challenging because of the radioresistance of recurrent tumors and the limited tolerance of the surrounding normal tissues. Particle therapy has demonstrated improved tumor control with superior sparing of adjacent organs. In this study, at equal biological doses, C-ions were significantly more effective than X-rays at suppressing tumor growth in HK-1 xenograft models, underscoring the therapeutic advantage of C-ions in reirradiation for treating recurrent NPC. However, CIRT is not widely accessible, and existing evidence indicates that reirradiation with C-ions still requires further optimization in terms of toxicity [1,5]. Effective radiosensitizers may offer a promising strategy for achieving a delicate balance between local tumor control and treatment-related toxicity minimization.

The radiosensitizing effects of PARPis have been observed in various types of tumors, and several phase I/II clinical trials have been conducted or are ongoing [35]. On the basis of the existing clinical results, while PARPis enhance the antitumor effect of radiotherapy, they also increase the level of acute toxicity in normal tissues within the target area. From this point of view, particle radiotherapy, with its superior dose distribution, may be more suitable for combination therapy with PARPis. In this study, we demonstrated that the PARP inhibitor olaparib effectively sensitizes recurrent NPC cells to both X-ray and C-ion radiation. Compared with either radiation type alone, the combination treatment resulted in better tumor regression in HK-1 xenograft models. With respect to HK-1, we established a more photon-resistant cell model, HK-RR, and found that olaparib also has significant radiosensitizing effects on these cells, suggesting its promising potential for enhancing the efficacy of reirradiation with either X-rays or C-ions for treating radioresistant recurrent NPC.

PARP1 plays a critical role in various aspects of DNA metabolism, including SSB repair, nucleotide excision repair, DSB repair, replication fork stabilization, and chromatin structure modulation [36]. In this study, we observed an accumulation of unrepaired DSBs following irradiation in the combined treatment group, which could be attributed to the impaired damage repair process and the conversion of accumulated, unrepairable SSBs into DSBs. Additionally, Sizemore *et al.* [33] reported that radiation induces BRCA1 cytoplasmic sequestration, leading to HR repair inhibition and subsequent sensitization to PARPis. Consistent with this finding, we used the HRD gene signature to functionally assess HR repair status and demonstrated that radiation exposure, particularly with C-ions, induces an HRD phenotype in HR-intact NPC cells. The hypothesis that IR sensitizes cells to PARPis is exciting, but the underlying molecular mechanisms require further validation.

Cells respond to DNA damage by activating complex signaling networks that influence cell fates, promoting DNA repair and survival while also triggering cell death [37]. Understanding the cell death pathways induced by antitumor treatments is crucial for optimizing treatment strategies, selecting appropriate patients and predicting patient prognoses. Radiation has been shown to induce multiple types of cell death, including apoptosis, necrosis, autophagy, ferroptosis, cuproptosis, senescence and mitotic catastrophe [38]. Importantly, the overall lethality of RT is not attributed to a single-cell death mechanism but rather to the cumulative effects of various pathways [39]. The contribution of each death pathway is influenced by the genetic background of the cell and the type and severity of damage. Therefore, evaluating the cytotoxic effect of radiation on the basis of a single death pathway may yield misleading results. Previous studies have highlighted the inconsistencies between apoptosis rates and clonogenic survival outcomes [40]. In the present study, both X-rays and C-ions were found to effectively induce apoptosis, necrosis, ferroptosis, ACD, and senescence in HK-1 cells. The differences between the cell death pathways of the two radiation types were not explored in this study. All the aforementioned pathways contribute to the cytotoxic effects of radiation combined with olaparib, with ACD being the predominant pathway.

Autophagy is a critical physiological process through which tumor cells respond to radiation-induced stress [41]. Following DNA damage or replication stress, increased autophagy plays dual roles, namely, providing energy and metabolic precursors to support damage repair and regulating the DNA damage response by selectively degrading pathway-specific proteins. Radiation-induced autophagy can be classified as cytoprotective or cytotoxic. In recent studies, researchers have proposed two additional categories, namely, cytostatic and nonprotective autophagy [42]. These classifications are primarily empirical and are determined by changes in cellular radiosensitivity following the pharmacological or genetic inhibition of autophagy, without the use of specific molecular markers. In our study, the autophagy induced by both X-rays and C-ions in HK-1 cells was cytotoxic or predominantly cytotoxic, and the radiosensitizing effect of olaparib relied on this cytotoxic autophagy.

DNA damage-induced autophagy controls the balance between cell survival and death [37]. The factors determining the direction in which this balance shifts remain unclear and are likely influenced by a combination of the cellular genetic background, the tumor microenvironment, and therapeutic interventions. Chakradeo *et al.* [43] proposed that the functional status of the p53 gene may influence the switch between protective and nonprotective autophagy induced by radiation. The inhibition of autophagy in p53 wild-type HN30 cells enhances radiosensitivity, indicating protective autophagy. However, in p53-mutant cells, including Hs578t, HN6, and H358 cells, pharmacological or genetic inhibition of autophagy has no effect on radiation sensitivity. Both the primary C666-1 NPC cell line (exon 7, codon 249 deletion) [44] and the recurrent HK-1 NPC cell line (c.388C>G, p.Leu130Val) harbor p53 mutations. Unfortunately, no other NPC cell lines are available because of HeLa contamination [45–47]. We conducted preliminary experiments using cervical cancer cell lines with various p53 statuses but did not

observe results that were fully consistent with those of Chakradeo *et al.* (data not shown), suggesting that p53 may not be the sole determinant of the role of autophagy. The conclusion derived from this study, *i.e.*, that ACD predominates in the cytotoxic effects of radiation combined with olaparib, may not universally apply to all cell lines. Further studies incorporating a broader range of cell lines with diverse genetic backgrounds are needed for validation purposes.

In conclusion, the PARP inhibitor olaparib has significant X-ray and C-ion radiosensitization effects on recurrent NPC cells and the associated HK-RR photon resistance model. A graphical abstract is presented in Supplementary Figure S6. Combining PARPis is a promising radiosensitization strategy for treating recurrent NPC in the future. The main limitations of the present study included the limited number of cell lines used and the lack of an in-depth exploration of the underlying molecular mechanisms. Additionally, the analysis did not encompass all possible cell death pathways. Given that most currently available NPC cell lines are contaminated with HeLa cells (Supplementary Data S1), there is an urgent need to develop new NPC cell lines derived from primary or recurrent tumors to facilitate further validation and exploration in future studies.

Supplementary Data

Supplementary data is available at *Acta Biochimica et Biphysica Sinica* online.

Funding

This work was supported by the grants from the Natural Science Foundation of China (No. 82103059) and the Science and Technology Development Fund of Shanghai Pudong New Area (No. PKJ2021-Y45).

Conflict of Interest

The authors declare that they have no conflict of interest.

References

1. Lee AWM, Ng WT, Chan JYW, Corry J, Mäkitie A, Mendenhall WM, Rinaldo A, *et al.* Management of locally recurrent nasopharyngeal carcinoma. *Cancer Treat Rev* 2019, 79: 101890
2. Ng WT, Lee MCH, Hung WM, Choi CW, Lee KC, Chan OSH, Lee AWM. Clinical outcomes and patterns of failure after intensity-modulated radiotherapy for nasopharyngeal carcinoma. *Int J Radiat Oncol Biol Phys* 2011, 79: 420–428
3. Tinganelli W, Durante M. Carbon ion radiobiology. *Cancers* 2020, 12: 3022
4. Wong KCW, Hui EP, Lo KW, Lam WKJ, Johnson D, Li L, Tao Q, *et al.* Nasopharyngeal carcinoma: an evolving paradigm. *Nat Rev Clin Oncol* 2021, 18: 679–695
5. Hu J, Huang Q, Gao J, Guan X, Hu W, Yang J, Qiu X, *et al.* Clinical outcomes of carbon-ion radiotherapy for patients with locoregionally recurrent nasopharyngeal carcinoma. *Cancer* 2020, 126: 5173–5183
6. Curtin NJ, Szabo C. Poly(ADP-ribose) polymerase inhibition: Past, present and future. *Nat Rev Drug Discov* 2020, 19: 711–736
7. Russo AL, Kwon HC, Burgan WE, Carter D, Beam K, Weizheng X, Zhang J, *et al.* *In vitro* and *in vivo* radiosensitization of glioblastoma cells by the poly (ADP-ribose) polymerase inhibitor E7016. *Clin Cancer Res* 2009, 15: 607–612
8. Laird JH, Lok BH, Ma J, Bell A, de Stanchina E, Poirier JT, Rudin CM. Talazoparib is a potent radiosensitizer in small cell lung cancer cell lines and xenografts. *Clin Cancer Res* 2018, 24: 5143–5152
9. Barreto-Andrade JC, Efimova EV, Mauceri HJ, Beckett MA, Sutton HG, Darga TE, Vokes EE, *et al.* Response of human prostate cancer cells and tumors to combining PARP inhibition with ionizing radiation. *Mol Cancer Ther* 2011, 10: 1185–1193
10. Verhagen CVM, de Haan R, Hageman F, Oostendorp TPD, Carli ALE, O'Connor MJ, Jonkers J, *et al.* Extent of radiosensitization by the PARP inhibitor olaparib depends on its dose, the radiation dose and the integrity of the homologous recombination pathway of tumor cells. *RadioTher Oncol* 2015, 116: 358–365
11. Césaire M, Ghosh U, Austry JB, Muller E, Cammarata FP, Guillamin M, Caruso M, *et al.* Sensitization of chondrosarcoma cells with PARP inhibitor and high-LET radiation. *J Bone Oncol* 2019, 17: 100246
12. Gilbert A, Tudor M, Delaunay A, Leman R, Levilly J, Atkinson A, Castéra L, *et al.* Radiosensitizing effect of PARP inhibition on chondrosarcoma and chondrocyte cells is dependent on radiation LET. *Biomolecules* 2024, 14: 1071
13. Dey P, Das R, Chatterjee S, Paul R, Ghosh U. Combined effects of carbon ion radiation and PARP inhibitor on non-small cell lung carcinoma cells: Insights into DNA repair pathways and cell death mechanisms. *DNA Repair* 2024, 144: 103778
14. Dong M, Luo H, Liu R, Zhang J, Yang Z, Wang D, Wang Y, *et al.* Radiosensitization of osteosarcoma cells using the PARP inhibitor olaparib combined with X-rays or carbon ions. *J Cancer* 2024, 15: 699–713
15. Chow JPH, Man WY, Mao M, Chen H, Cheung F, Nicholls J, Tsao SW, *et al.* PARP1 is overexpressed in nasopharyngeal carcinoma and its inhibition enhances radiotherapy. *Mol Cancer Ther* 2013, 12: 2517–2528
16. Huang DP, Ho JHC, Poon YF, Chew EC, Saw D, Lui M, Li CL, *et al.* Establishment of a cell line (NPC/HK1) from a differentiated squamous carcinoma of the nasopharynx. *Intl J Cancer* 1980, 26: 127–132
17. Zhou ZR, Wang XY, Yu XL, Mei X, Chen XX, Hu QC, Yang ZZ, *et al.* Building radiation-resistant model in triple-negative breast cancer to screen radioresistance-related molecular markers. *Ann Transl Med* 2020, 8: 108
18. Li H, Durbin R. Fast and accurate short read alignment with Burrows–Wheeler transform. *Bioinformatics* 2009, 25: 1754–1760
19. McKenna A, Hanna M, Banks E, Sivachenko A, Cibulskis K, Kernytsky A, Garimella K, *et al.* The Genome Analysis Toolkit: a MapReduce framework for analyzing next-generation DNA sequencing data. *Genome Res* 2010, 20: 1297–1303
20. Wang K, Li M, Hakonarson H. ANNOVAR: Functional annotation of genetic variants from high-throughput sequencing data. *Nucleic Acids Res* 2010, 38: e164
21. Richards S, Aziz N, Bale S, Bick D, Das S, Gastier-Foster J, Grody WW, *et al.* Standards and guidelines for the interpretation of sequence variants: a joint consensus recommendation of the American College of Medical Genetics and Genomics and the Association for Molecular Pathology. *Genet Med* 2015, 17: 405–424
22. Le Z, Niu X, Chen Y, Ou X, Zhao G, Liu Q, Tu W, *et al.* Predictive single nucleotide polymorphism markers for acute oral mucositis in patients with nasopharyngeal carcinoma treated with radiotherapy. *Oncotarget* 2017, 8: 63026–63037
23. Nomiya T. Discussions on target theory: past and present. *J Radiat Res* 2013, 54: 1161–1163
24. Martins I, Raza SQ, Voisin L, Dakhli H, Allouch A, Law F, Sabino D, *et al.* Anticancer chemotherapy and radiotherapy trigger both non-cell-autonomous and cell-autonomous death. *Cell Death Dis* 2018, 9: 716
25. Sosna J, Voigt S, Mathieu S, Lange A, Thon L, Davarnia P, Herdegen T, *et al.* TNF-induced necroptosis and PARP-1-mediated necrosis represent

distinct routes to programmed necrotic cell death. *Cell Mol Life Sci* 2014, 71: 331–348
26. Stockwell BR. Ferroptosis turns 10: emerging mechanisms, physiological functions, and therapeutic applications. *Cell* 2022, 185: 2401–2421
27. Bolger AM, Lohse M, Usadel B. Trimmomatic: a flexible trimmer for Illumina sequence data. *Bioinformatics* 2014, 30: 2114–2120
28. Kim D, Paggi JM, Park C, Bennett C, Salzberg SL. Graph-based genome alignment and genotyping with HISAT2 and HISAT-genotype. *Nat Biotechnol* 2019, 37: 907–915
29. Liao Y, Smyth GK, Shi W. featureCounts: an efficient general purpose program for assigning sequence reads to genomic features. *Bioinformatics* 2014, 30: 923–930
30. Peng G, Chun-Jen Lin C, Mo W, Dai H, Park YY, Kim SM, Peng Y, ***et al.*** Genome-wide transcriptome profiling of homologous recombination DNA repair. *Nat Commun* 2014, 5: 3361
31. Lyu F, Han F, Ge C, Mao W, Chen L, Hu H, Chen G, ***et al.*** OmicStudio: a composable bioinformatics cloud platform with real-time feedback that can generate high-quality graphs for publication. *iMeta* 2023, 2: e85
32. Shen W, Song Z, Zhong X, Huang M, Shen D, Gao P, Qian X, ***et al.*** Sangerbox: a comprehensive, interaction-friendly clinical bioinformatics analysis platform. *iMeta* 2022, 1: e36
33. Sizemore ST, Mohammad R, Sizemore GM, Nowsheen S, Yu H, Ostrowski MC, Chakravarti A, ***et al.*** Synthetic lethality of PARP inhibition and ionizing radiation is p53-dependent. *Mol Cancer Res* 2018, 16: 1092–1102
34. Borges HL, Linden R, Wang JY. DNA damage-induced cell death: lessons from the central nervous system. *Cell Res* 2008, 18: 17–26
35. Barcellini A, Loap P, Murata K, Villa R, Kirova Y, Okonogi N, Orlandi E. PARP inhibitors in combination with radiotherapy: to do or not to do? *Cancers* 2021, 13: 5380
36. Ray Chaudhuri A, Nussenzweig A. The multifaceted roles of PARP1 in DNA repair and chromatin remodelling. *Nat Rev Mol Cell Biol* 2017, 18: 610–621
37. Roos WP, Thomas AD, Kaina B. DNA damage and the balance between survival and death in cancer biology. *Nat Rev Cancer* 2016, 16: 20–33
38. Chen H, Han Z, Luo Q, Wang Y, Li Q, Zhou L, Zuo H. Radiotherapy modulates tumor cell fate decisions: a review. *Radiat Oncol* 2022, 17: 196
39. Surova O, Zhivotovsky B. Various modes of cell death induced by DNA damage. *Oncogene* 2013, 32: 3789–3797
40. Abend M. Reasons to reconsider the significance of apoptosis for cancer therapy. *Int J Radiat Biol* 2003, 79: 927–941
41. Juretschke T, Beli P. Causes and consequences of DNA damage-induced autophagy. *Matrix Biol* 2021, 100-101: 39–53
42. Gewirtz DA. The four faces of autophagy: implications for cancer therapy. *Cancer Res* 2014, 74: 647–651
43. Chakradeo S, Sharma K, Alhaddad A, Bakhshwin D, Le N, Harada H, Nakajima W, ***et al.*** Yet another function of p53—the switch that determines whether radiation-induced autophagy will be cytoprotective or nonprotective: implications for autophagy inhibition as a therapeutic strategy. *Mol Pharmacol* 2015, 87: 803–814
44. Syn NL, Lim PL, Kong LR, Wang L, Wong ALA, Lim CM, Loh TKS, ***et al.*** Pan-CDK inhibition augments cisplatin lethality in nasopharyngeal carcinoma cell lines and xenograft models. *Sig Transduct Target Ther* 2018, 3: 9
45. Capes-Davis A, Theodosopoulos G, Atkin I, Drexler HG, Kohara A, MacLeod RA, Masters JR, ***et al.*** Check your cultures! A list of cross-contaminated or misidentified cell lines. *Int J Cancer* 2010, 127: 1–8
46. Chan SY, Choy KW, Tsao SW, Tao Q, Tang T, Chung GT, Lo KW. Authentication of nasopharyngeal carcinoma tumor lines. *Int J Cancer* 2008, 122: 2169–2171
47. Strong MJ, Baddoo M, Nanbo A, Xu M, Puetter A, Lin Z, Longnecker RM. Comprehensive high-throughput RNA sequencing analysis reveals contamination of multiple nasopharyngeal carcinoma cell lines with hela cell genomes. *J Virol* 2014, 88: 10696–10704